

Constraints of Flat Spectrum Radio Quasars in the hadronic model: the case of 3C 273

M. Petropoulou^{1*} † & S. Dimitrakoudis²

¹*Department of Physics and Astronomy, Purdue University, 525 Northwestern Avenue, West Lafayette, IN 47907, USA*

²*Institute for Astronomy, Astrophysics, Space Applications & Remote Sensing, National Observatory of Athens, 15 236 Penteli, Greece*

Received / Accepted

ABSTRACT

We present a method of constraining the properties of the γ -ray emitting region in flat spectrum radio quasars (FSRQs) in the one-zone proton synchrotron model, where the γ -rays are produced by synchrotron radiation of relativistic protons. We show that for low enough values of the Doppler factor δ , the emission from the electromagnetic (EM) cascade which is initiated by the internal absorption of high-energy photons from photohadronic interactions may exceed the observed \sim GeV flux. We use that effect to derive an absolute lower limit of δ ; first, an analytical one, in the asymptotic limit where the external radiation from the broad line region (BLR) is negligible, and then a numerical one in the more general case that includes BLR radiation. As its energy density in the emission region depends on δ and the region's distance from the galactic center, we use the EM cascade to determine a minimum distance for each value of δ . We complement the EM cascade constraint with one derived from variability arguments and apply our method to the FSRQ 3C 273. We find that $\delta \gtrsim 18 - 20$ for $B \lesssim 30$ G and \sim day timescale variability; the emission region is located outside the BLR, namely at $r \gtrsim 10R_{\text{BLR}} \sim 3$ pc; the model requires at pc-scale distances stronger magnetic fields than those inferred from core shift observations; while the jet power exceeds by at least one order of magnitude the accretion power. In short, our results disfavour the proton synchrotron model for the FSRQ 3C 273.

Key words: astroparticle physics – radiation mechanisms: non-thermal – galaxies: active: individual: 3C 273

1 INTRODUCTION

Blazars are a class of Active Galactic Nuclei (AGN), whose broad-band photon spectrum is dominated by non-thermal emission. This is believed to be produced within a relativistic jet oriented at a small angle with respect to the line of sight (Blandford & Rees 1978; Urry & Padovani 1995). The spectral energy distribution (SED) of blazars is comprised of two broad non-thermal components: a low-energy one, that extends from the radio up to the UV or X-ray frequency range, and a high-energy one that covers the X-ray and γ -ray energy bands (Padovani & Giommi 1995; Fossati et al. 1998).

It is commonly believed that the low-energy blazar emission is the result of electron synchrotron radiation, with the peak frequency reflecting the maximum energy at which electrons can be accelerated (e.g. Giommi et al. 2012). However, the origin of their high-energy emission has not been yet settled. Among the proposed mechanisms for γ -ray production in blazars are: synchrotron self-Compton radiation (e.g. Maraschi et al. 1992; Bloom & Marscher 1996; Mastichiadis & Kirk 1997), ex-

ternal Compton scattering (e.g. Dermer et al. 1992; Sikora et al. 1994; Ghisellini & Madau 1996), proton synchrotron radiation (Aharonian 2000; Mücke & Protheroe 2001), and photohadronic interactions (e.g. Mannheim & Biermann 1992; Atayan & Dermer 2001; Petropoulou et al. 2015). For Flat Spectrum Radio Quasars (FSRQs) in particular, which are characterized by large values of the so-called “Compton dominance”, i.e. large ratios of the peak high-energy luminosity to the low-energy one, the SSC scenario is disfavoured, while the EC and proton synchrotron scenarios remain viable (e.g. Sikora et al. 2009; Chatterjee et al. 2013; Böttcher et al. 2013). Besides the radiative process responsible for the blazar high-energy emission, the distance of the emission region from the super-massive black hole that lies in the galactic center (sub-pc vs. pc scale), remains a matter of debate (e.g. Błażejowski et al. 2000; Tavecchio et al. 2010; Poutanen & Stern 2010; Marscher et al. 2012; Stern & Poutanen 2014). In the case of FSRQs, the presence of external photon fields may be used to constrain the location of the γ -ray emission region, at least within the leptonic EC scenario (see e.g. Nalewajko et al. 2014).

In leptonic models the external radiation field has a primary role in the formation of the SED, as it provides the seeds for inverse Compton scattering in the γ -ray regime. In leptohadronic

* E-mail: mpetropo@purdue.edu

† Einstein Postdoctoral Fellow

models though, the role of external photons in producing the observed SED is not straightforward. Besides the internally produced low-energy synchrotron photons, external photons, e.g. from the Broad Line Region (BLR), act as additional targets for photohadronic interactions with the accelerated protons. In particular, if the emission region is located within the BLR, its energy density as measured in the respective comoving frame will appear boosted, thus increasing the efficiency of photopion production. It is noteworthy that FSRQs have been suggested as promising sites of PeV neutrino emission (e.g. Atoyan & Dermer 2001; Stecker 2013; Murase et al. 2014; ANTARES Collaboration et al. 2015). Given the recent detection of high-energy astrophysical neutrinos (IceCube Collaboration 2013; Aartsen et al. 2014), leptonhadronic models pose an attractive alternative to leptonic scenarios for blazar emission (e.g. Halzen & Zas 1997).

In this study, we present a method for constraining the Doppler factor and the location of the high-energy emission region in FSRQs within the proton synchrotron scenario (for constraints in the leptonic scenario of blazar emission, see e.g. Dondi & Ghisellini 1995; Rani et al. 2013; Nalewajko et al. 2014; Zacharias 2015). Our method is based on the effects of the unavoidable, additional emission produced through photohadronic interactions, namely via Bethe-Heitler pair production and photopion production. In addition to the γ -ray photons produced by neutral pion (π^0) decay, both channels of photohadronic interactions lead to the injection of highly relativistic electron/positron pairs¹, that will contribute to the photon spectrum as well. Depending on the parameters that describe the emission region, such as its size and the magnetic field strength, secondary pairs lose energy preferentially through synchrotron or inverse Compton processes, and their emission signatures may appear on the SED (see e.g. Petropoulou & Mastichiadis 2015). For the case of FSRQs, their emission emerges typically at energies much higher than the peak of the high-energy component of the SED, and is also subjected to intrinsic photon-photon absorption (Dermer et al. 2007). If the optical depth for intrinsic photon-photon absorption ($\tau_{\gamma\gamma}$) is much larger than unity, then an electromagnetic (EM) cascade will be initiated, transferring energy to the GeV-TeV energy range; it may even dominate over the proton synchrotron emission (e.g. Mannheim et al. 1991) and, in such a case, the SED may no longer resemble that of a typical FSRQ.

An important quantity in our study is the photon/particle compactness, which is a dimensionless measure of the photon/particle energy density. It is usually expressed as $\ell \propto L/R$, where L and R are, respectively, the comoving luminosity and size of the emission region. Roughly speaking, higher compactnesses of the internally produced synchrotron photons, of the external photons, and of the primary injected protons, result in higher photohadronic production rates and higher optical depths $\tau_{\gamma\gamma}$ (see also Dermer et al. 2007). This is another manifestation of the so-called “compactness problem” in blazars: the photon compactness in the γ -ray emission region of a blazar cannot become arbitrarily high because of the initiated EM cascades that deform its multi-wavelength emission². Since there are different combinations of the Doppler factor and of the compactness of primary particles that result in the same observed flux, it follows that the choice of low Doppler factor values favours higher production rates of secondary pairs and higher $\tau_{\gamma\gamma}$.

By reversing the aforementioned argument, it is evident that for a given observed γ -ray flux, size, magnetic field strength and photon compactness, there is a minimum Doppler factor value that can be well defined. Taking into account that the total (internal and external) photon compactness depends, in turn, on the location of the emission region in the blazar jet, we can define, for each Doppler factor value, a minimum distance as well.

This paper is structured as follows. In Sect. 2 we derive an analytical expression of the minimum Doppler factor in the limiting case where the internal photon compactness is much larger than the external one; this sets the most stringent limit on the Doppler factor. In Sect. 3 we present the model and the algorithm for the numerical determination of minimum distance of the emission region. We present the results of our method when applied to the FSRQ 3C 273 in Sect. 4, and discuss other possible constraints. We continue in Sect. 5 with a discussion of our results and conclude in Sect. 6.

2 ANALYTICAL APPROACH

The existence of a minimum Doppler factor (δ_{\min}) in the proton synchrotron model for blazar emission can be demonstrated with analytical arguments. In doing so, we will also derive an analytical expression that will reveal its dependence on the quantities describing the blazar emission region. Our analysis will be focused on the minimal case where the internally produced synchrotron photons are the only targets for photohadronic interactions; this is also the case of minimum photon compactness and may be realizable if the emitting region is located much further out of the region of external radiation (see Fig. 2).

We approximate the electron synchrotron differential luminosity as a broken power-law:

$$L'_s(\epsilon') = A_1 \epsilon'^{-\beta_1} H[\epsilon'_s - \epsilon'] + A_2 \epsilon'^{-\beta_2} H[\epsilon' - \epsilon'_s], \quad (1)$$

where $H[x] = 1$ for $x > 0$ and 0 otherwise. From this point on, we use the following convention: primed and unprimed quantities are measured in the comoving frame of the emission region and in the observer’s frame, respectively. The normalization constants are

$$A_2 = A_1 \epsilon_s'^{\beta_2 - \beta_1} \quad (2)$$

$$A_1 = \frac{(1 - \beta_1)(\beta_2 - 1)}{\beta_2 - \beta_1} \epsilon_s'^{\beta_1 - 1} L'_s. \quad (3)$$

where $\beta_2 > 1$, $\beta_1 < 1$, $L'_s = L_s/\delta^4$ is the total synchrotron luminosity, and $\epsilon'_s = \epsilon_s(1 + z)/\delta$ is the break energy of the synchrotron spectrum, which for the particular choice of spectral indices coincides with the synchrotron peak energy.

The differential number density of synchrotron photons is written as

$$n'_s(\epsilon') = \tilde{A}_1 \epsilon'^{-\Gamma_1} H[\epsilon'_s - \epsilon'] + \tilde{A}_2 \epsilon'^{-\Gamma_2} H[\epsilon' - \epsilon'_s], \quad (4)$$

where $\Gamma_1 = \beta_1 + 1$ and $\Gamma_2 = \beta_2 + 1$ are the low- and high-energy photon indices, respectively, and

$$\tilde{A}_{1,2} = \frac{3}{4\pi c R^2} A_{1,2}. \quad (5)$$

The optical depth for the absorption of γ -ray photons with energy ϵ'_1 is

$$\tau_{\gamma\gamma}(\epsilon'_1) \simeq \frac{R \sigma_0 (m_e c^2)^2}{\epsilon'_1} \int_{2(m_e c^2)^2/\epsilon'_1}^{\infty} d\epsilon' \frac{n'_s(\epsilon')}{\epsilon'} \quad (6)$$

¹ From this point on we refer to them commonly as ‘electrons’.

² This has been also pointed out in (Petropoulou & Mastichiadis 2012) for the case where no soft photons are initially present in the region (automatic photon quenching).

where we approximated the photon-photon absorption cross section as³ $\sigma_{\gamma\gamma}(x_1, x) \approx \sigma_0 H[x_1 x - 2]/(x_1 x)$ (Coppi & Blandford 1990). Here, x_1, x are the photon energies in units of $m_e c^2$ and $\sigma_0 = 0.652\sigma_T$. For $\epsilon'_s \epsilon'_1 \gtrsim 2(m_e c^2)^2$ the integral simplifies into

$$\tau_{\gamma\gamma}(\epsilon_1) \approx \frac{3\sigma_0 f(\beta_1, \beta_2)}{8\pi c R \delta^3 (1+z)} \frac{L_s}{\epsilon_s} \left(\frac{\epsilon_s \epsilon_1 (1+z)^2}{2(m_e c^2)^2 \delta^2} \right)^{\beta_1}, \quad (7)$$

where

$$f = \frac{(1-\beta_1)(\beta_2-1)}{(\beta_2-\beta_1)(1+\beta_1)}. \quad (8)$$

The γ -rays produced through π^0 decay are, in principal, very energetic and can easily satisfy the threshold criterion for photon-photon absorption on the synchrotron photons with energy ϵ'_s . This can be understood as follows. In the proton synchrotron model, the high-energy component of the blazar SED is explained as synchrotron radiation of relativistic protons. The maximum proton Lorentz factor is related to the peak frequency (ν_γ) of the γ -ray spectrum as

$$\gamma_{p,\max} = \left(\frac{2\pi(1+z)\nu_\gamma m_p c}{q_e B \delta} \right)^{1/2} \quad (9)$$

or, using indicative parameter values,

$$\gamma_{p,\max} = 2.4 \times 10^8 (B_1 \delta_1)^{-1/2} ((1+z)\nu_{\gamma,22})^{1/2}, \quad (10)$$

where we introduced the notation $q_x \equiv q/10^x$ in cgs units. The typical energy of γ -ray photons produced by neutral pion decay is $\epsilon'_{\pi^0 \rightarrow 2\gamma} \simeq 0.5 \kappa_{p\pi} m_p \gamma_p c^2$ where $\kappa_{p\pi} \simeq 0.2$ is the mean proton inelasticity; in fact, the inelasticity increases from $\sim m_\pi/m_p (\simeq 0.14)$ close to the threshold to ~ 0.5 at an energy three times larger than the threshold one (Stecker 1968; Begelman et al. 1990). Thus, protons with Lorentz factor $\gamma_{p,\max}$ result in the production of very high-energy photons:

$$\epsilon'_{\pi^0 \rightarrow 2\gamma} \simeq 2.4 \times 10^4 \text{ TeV } (B_1 \delta_1)^{-1/2} ((1+z)\nu_{\gamma,22})^{1/2}. \quad (11)$$

For a fiducial synchrotron peak energy $\epsilon_s = 0.1 \text{ eV}$, which corresponds to

$$\epsilon'_s = 0.01 \text{ eV } \frac{(1+z)}{\delta_1} \frac{\epsilon_s}{0.1 \text{ eV}}, \quad (12)$$

we find that $\epsilon'_{\pi^0 \rightarrow 2\gamma} \epsilon'_s \gg 2(m_e c^2)^2$. By substitution of eqs. (11) and (12) in eq. (7) we find the respective optical depth to be

$$\tau_{\gamma\gamma}(\epsilon_{\pi^0 \rightarrow 2\gamma}) \simeq \frac{4 \times 10^3}{(1+z)} \left(\frac{0.1 \text{ eV}}{\epsilon_s} \right)^{1/2} \frac{L_{s,45}}{R_{16} \delta_1^3} \left(\frac{1+z}{\delta_1} \right)^{3/4} \left(\frac{\nu_{\gamma,22}}{B_1} \right)^{1/4}, \quad (13)$$

where we assumed $\beta_1 = 1/2$ and $\beta_2 = 3/2$. Since $\tau_{\gamma\gamma}(\epsilon_{\pi^0 \rightarrow 2\gamma}) \gg 1$ is typical, the γ -ray luminosity from π^0 decay ($L_{\pi^0 \rightarrow 2\gamma}$) will be totally absorbed. We may thus write that $L_{\pi^0 \rightarrow 2\gamma}^{\text{abs}} = (1 - e^{-\tau_{\gamma\gamma}}) L_{\pi^0 \rightarrow 2\gamma} \simeq L_{\pi^0 \rightarrow 2\gamma}$. The absorbed photon luminosity will be re-distributed at lower γ -ray energies through the development of an EM cascade. This emerges as an additional emission that should be below the proton synchrotron component, which in our framework is responsible for the FSRQ high-energy emission.

We note that photons emitted by secondary, highly relativistic electrons from charged (π^+) pion decay or/and Bethe-Heitler pair production are also subject to photon-photon absorption, and thus they may contribute to the cascade emission. The synchrotron photons emitted by secondary pairs are less energetic than those from

π^0 decays. Thus, they are mainly attenuated by photons with energies $\epsilon' \gtrsim \epsilon'_s$. To exemplify this, let us consider the most energetic pairs produced by pion decays. These are produced roughly with $\gamma_{p\pi} \simeq (1/4) \kappa_{p\pi} \gamma_{p,\max} m_p / m_e$, and the respective synchrotron photon energy is written as

$$\epsilon'_{s,p\pi} \simeq 60 \text{ TeV } \delta_1^{-1} (1+z) \nu_{\gamma,22}. \quad (14)$$

This lies just above the threshold for $\gamma\gamma$ absorption on photons with ϵ'_s . Cooling of pairs with $\gamma_{p\pi}$ as well as the production of pairs from protons with $\gamma_p < \gamma_{p,\max}$ results in photon emission at $\epsilon' \ll \epsilon'_{s,p\pi}$, where the threshold condition for absorption on ϵ'_s is no more satisfied. Since $n'_s \propto \epsilon'^{-1-\beta_2}$ for $\epsilon' > \epsilon'_s$, the optical depth for absorption of photons with $\epsilon' \ll \epsilon'_{s,p\pi}$ is expected to be much less than

$$\tau_{\gamma\gamma}(\epsilon'_{s,p\pi}) \simeq \frac{10^2}{(1+z)} \left(\frac{0.1 \text{ eV}}{\epsilon_s} \right) \frac{L_{s,45}}{R_{16} \delta_1^3}, \quad (15)$$

where we used eqs. (14), (6) and $\epsilon'_s \epsilon'_{s,p\pi} \approx 2(m_e c^2)^2$. Moreover, the synchrotron spectrum from pairs spans many decades in energy and the luminosity emitted at $\epsilon'_{s,p\pi}$ is, therefore, only a fraction of the total injected luminosity in pairs. This is not the case for the γ -ray spectrum from π^0 decays, which is sharply peaked at $\epsilon'_{\pi^0 \rightarrow 2\gamma}$. Similar arguments apply to the synchrotron emission from Bethe-Heitler pairs, which are produced on average with $\gamma < \gamma_{p\pi}$. Thus, for the purposes of this analytical approach, we can safely ignore the attenuation of photons from Bethe-Heitler and pion decay process, and consider only the attenuation of γ -ray photons from π^0 decay. In any case, our analytical results will be compared against those calculated numerically, after taking into account the additional photon emission from Bethe-Heitler and charged pion processes (see Sect. 4).

Since the proton synchrotron emission alone can explain the observed γ -ray spectrum, the sum of the cascade and proton synchrotron emission may exceed the observations for high enough values of $L_{\pi^0 \rightarrow 2\gamma}$. This can be avoided if the following energetic constraint is satisfied

$$L_{\pi^0 \rightarrow 2\gamma}^{\text{abs}} \lesssim \eta L_{\gamma,\text{pk}}, \quad (16)$$

where $L_{\gamma,\text{pk}}$ is the peak luminosity of the high-energy SED component, which is typically a good proxy of the total γ -ray luminosity. Here, $\eta \lesssim 1$ is a dimensionless factor to be defined later by the observations (see Sect. 4). The above relation does not take into account any spectral information about the developed EM cascade (e.g. Mannheim 1993; Petropoulou et al. 2013). It is based on the simplifying assumption that the absorbed luminosity re-emerges at the energy where $\tau_{\gamma\gamma}(\epsilon_*) \sim 1$. Using fiducial parameter values and solving eq. (7) for ϵ_* , we find

$$\epsilon_* \simeq 18 \text{ GeV } \frac{\epsilon_s}{0.1 \text{ eV}} \delta_1^8 L_{s,45}^{-2} R_{16}^2, \quad (17)$$

where we also assumed $\beta_1 = 1/2$ and $\beta_2 = 3/2$. We thus expect the EM cascade to emerge at energies higher than the peak of the high-energy emission, which for FSRQs usually falls in the 4 MeV–40 MeV (10^{21} Hz– 10^{22} Hz) range (Fossati et al. 1998). The constraint imposed by relation (16) could be relaxed if we were to include spectral information for the cascade emission. However, this lies out of the scope of the present work.

The γ -ray luminosity from the π^0 decay may be written as

$$L_{\pi^0 \rightarrow 2\gamma}^{\text{abs}} \simeq L_{\pi^0 \rightarrow 2\gamma} \simeq 2 \times \frac{1}{2} \tau_{p\pi} L_p, \quad (18)$$

where $\tau_{p\pi}$ is the optical depth for photopion interactions (to be defined below) and L_p is the total injected proton luminosity. The factors 2 and 1/2 account for the production of two photons that share

³ For simplifying reasons, we neglected the logarithmic dependence.

the energy of the parent neutral pion. In what follows, we will use eqs. (16) and (18) for deriving and justifying the existence of a minimum Doppler factor.

Before we calculate the optical depth for photopion ($p\pi$) interactions, it is useful to determine the threshold photon energy for such interactions with protons having Lorentz factor $\gamma_{p,\max}$. Using eq. (10) we find

$$\epsilon'_{\text{th}} \simeq 0.58 \text{ eV} (B_1 \delta_1)^{1/2} \left((1+z) \nu_{\gamma,22} \right)^{-1/2}, \quad (19)$$

which for typical parameter values, is $\epsilon'_{\text{th}} \gg \epsilon'_s$ (see also eq. (12)). Lower energy protons will interact with synchrotron photons of energy $\epsilon' > \epsilon'_{\text{th}}$, whose number density decreases as $\propto \epsilon'^{-1-\beta_2}$; we will not consider these interactions in the following.

The optical depth for $p\pi$ interactions is defined as $\tau_{p\pi}(\gamma_p) \equiv t_{\text{cr}}/t_{p\pi}(\gamma_p)$, where $t_{\text{cr}} = R/c$ and $t_{p\pi}^{-1}$ is the $p\pi$ energy loss rate given by (Stecker 1968)

$$t_{p\pi}^{-1}(\gamma_p) \approx \frac{c}{2\gamma_p^2} \int_{\bar{\epsilon}_{\text{th}}}^{\infty} d\bar{\epsilon} \bar{\epsilon} \sigma_{p\pi}(\bar{\epsilon}) \kappa_{p\pi}(\bar{\epsilon}) \int_{\bar{\epsilon}/2\gamma_p}^{\infty} d\epsilon' \frac{n'(\epsilon')}{\epsilon'^2}, \quad (20)$$

where $\bar{\epsilon}_{\text{th}} = 145 \text{ MeV}$. We assume $\kappa_{p\pi}(\bar{\epsilon}) \approx 0.2$ and approximate the cross section as $\sigma_{p\pi} = \bar{\sigma}_{p\pi} H[\bar{\epsilon} - \bar{\epsilon}_{\text{th}}]$, where $\bar{\sigma}_{p\pi} = 1.5 \times 10^{-4} \sigma_T$ (for a more realistic description of $\sigma_{p\pi}$, see Mücke et al. 2000; Beringer et al. 2012). For the photon spectrum defined by eq. (4), the second integral is written as

$$\int_{\bar{\epsilon}/2\gamma_p}^{\infty} d\epsilon' \frac{n'(\epsilon')}{\epsilon'^2} = \int_{\bar{\epsilon}/2\gamma_p}^{\epsilon'_s} d\epsilon' \tilde{A}_1 \epsilon'^{-3-\beta_1} + \int_{\max[\bar{\epsilon}/2\gamma_p, \epsilon'_s]}^{\infty} d\epsilon' \tilde{A}_2 \epsilon'^{-3-\beta_2}. \quad (21)$$

For the highest energy protons, i.e. with Lorentz factor $\gamma_{p,\max}$, only the second integral is non-zero, and the respective optical depth is written as

$$\tau_{p\pi}(\gamma_{p,\max}) \simeq \frac{3\bar{\sigma}_{p\pi} \kappa_{p\pi}}{2\pi c R} \frac{L_s}{\epsilon_s} \frac{g(\beta_2, \beta_1)}{\delta^3 (1+z)} \left(\frac{2\gamma_{p,\max} \epsilon_s (1+z)}{\delta \bar{\epsilon}_{\text{th}}} \right)^{\beta_2} \quad (22)$$

where

$$g(\beta_2, \beta_1) = \frac{(1-\beta_1)(\beta_2-1)}{\beta_2(\beta_2-\beta_1)(2+\beta_2)}. \quad (23)$$

Using eq. (10), $\beta_1 = 1/2$, $\beta_2 = 3/2$ and fiducial values for the other parameters, the optical depth is written as

$$\tau_{p\pi}(\gamma_{p,\max}) \simeq 6 \times 10^{-5} \frac{L_{s,45} \nu_{\gamma,22}^{3/4}}{R_{16} B_1^{3/4} \delta_1^{21/4} (1+z)^{1/4}} \left(\frac{\epsilon_s}{0.1 \text{ eV}} \right)^{1/2}. \quad (24)$$

Using the approximation $L_{\gamma,\text{pk}} \approx L_\gamma$, the definition of the proton compactness ℓ_p , which is a dimensionless measure of the proton luminosity, given by

$$\ell_p = \frac{\sigma_T L_p}{4\pi R m_p c^3 \delta^4}, \quad (25)$$

and eqs. (16), (18) and (22) we find that

$$6g(\beta_2, \beta_1) \frac{\bar{\sigma}_{p\pi} \kappa_{p\pi}}{\sigma_T} \frac{L_s}{\eta L_\gamma} (\epsilon_s (1+z))^{\beta_2-1} \left(\frac{2\gamma_{p,\max}}{\bar{\epsilon}_{\text{th}}} \right)^{\beta_2} \ell_p m_p c^2 \delta^{1-\beta_2} \lesssim 1. \quad (26)$$

At this point, we make use of our working hypothesis, namely that the γ -ray emission is explained by proton synchrotron radiation. Using standard expressions for the synchrotron luminosity emitted by a power-law proton distribution (e.g. eq. (6.36) in Rybicki & Lightman (1986)) we may express ℓ_p as

$$\ell_p = \frac{C_p \sigma_T L_\gamma B^{-(p+1)/2} \delta^{-(p+5)/2}}{4\pi R^2 f_p \nu_\gamma^{(3-p)/2}} \quad (27)$$

where $f_p = (p-2)/(p-1)$ with $p \neq 1$ being the power-law index

of the injected proton distribution and

$$C_p = \frac{(3-p)(p+1)(2\pi)^{(p-1)/2} m_p^{(p+1)/2} c^{(p+3)/2}}{2q_e^{(5+p)/2} 3^{p/2} \Gamma_1(p) \Gamma_2(p)} \quad (28)$$

$$\Gamma_1 = \Gamma\left(\frac{p}{4} + \frac{19}{12}\right) \quad (29)$$

$$\Gamma_2 = \Gamma\left(\frac{p}{4} - \frac{1}{12}\right), \quad (30)$$

where $\Gamma(t) \equiv \int_0^\infty dx x^{t-1} e^{-x}$. The constant C_p^{-1} is a generalization of C_2 given by eq. (9) in Petropoulou & Mastichiadis (2012) for $2 < p < 3$. Substitution of eqs. (10) and (27) into eq. (26) results in

$$\delta \gtrsim \delta_{\min}, \quad (31)$$

with

$$\delta_{\min}^{(p+3+3\beta_2)/2} \simeq C_1 L_s \eta^{-1} R^{-2} \epsilon_s^{\beta_2-1} \nu_\gamma^{(\beta_2+p-3)/2} B^{-(\beta_2+p+1)/2}. \quad (32)$$

In the above,

$$C_1 = \frac{6}{4\pi} g(\beta_2, \beta_1) \bar{\sigma}_{p\pi} \kappa_{p\pi} m_p c^2 C_p \frac{f_z^{3\beta_2/2}}{f_z f_p} \left(\frac{2}{\bar{\epsilon}_{\text{th}}} \right)^{\beta_2} \left(\frac{2\pi m_p c}{q_e} \right)^{\beta_2/2} \quad (33)$$

and $f_z \equiv 1+z$. It is noteworthy that δ_{\min} does not depend on the γ -ray luminosity, while it has a weak dependence on most of other model parameters:

$$\delta_{\min} \propto R^{-1/w} \eta^{-2/w} L_s^{2/w} \epsilon_s^{2(\beta_2-1)/w} \nu_\gamma^{(\beta_2+p-3)/w} B^{-(p+1+\beta_2)/w}, \quad (34)$$

where $w = p+3+3\beta_2$. Instead, the strongest dependence comes through the magnetic field strength and the spectral index of the synchrotron spectrum above its peak:

- the minimum Doppler factor decreases for stronger magnetic fields. Higher values of B require lower proton luminosity to explain a given observed γ -ray luminosity, as eq. (27) demonstrates. This subsequently reduces the luminosity produced through photohadronic interactions and, thus, the amount of energy being absorbed and reprocessed (see eq. (18));

- the minimum Doppler factor decreases as the electron synchrotron spectrum above its peak becomes steeper. This can be easily understood, since the respective number density of synchrotron photons scales as $n'_s(\epsilon') \propto \epsilon'^{-1-\beta_2}$ and decreases for higher β_2 . We remind that very high energy γ -rays produced via photohadronic interactions are mostly absorbed by these synchrotron photons.

The dependence of δ_{\min} on the magnetic field strength is exemplified in Fig. 1, where δ_{\min} is shown as a function of B for two values of the emission region radius: $R = 3.6 \times 10^{16} \text{ cm}$ (solid line) and $3.6 \times 10^{15} \text{ cm}$ (dashed line). Other parameters used for the plot are: $\nu_s = \epsilon_s/h = 3.2 \times 10^{13} \text{ Hz}$, $L_s = 6.3 \times 10^{45} \text{ erg/s}$ (this corresponds to 10^{13} Jy Hz for the 3C 273 distance $D_L = 755 \text{ Mpc}$), $\nu_\gamma = 10^{22} \text{ Hz}$, $\eta = 0.2$, $p = 2.3$, $\beta_1 = 0.7$ and $\beta_2 = 1.35$. Our choice of the parameter values is motivated by the SED fitting of 3C 273 (see Sect. 4).

Figure 1 demonstrates that the Doppler factor of the high-energy emission region in FSRQs lies above 15-20, unless the magnetic field strength is high, i.e. $\gtrsim 30 \text{ G}$ and/or the synchrotron photon spectrum is steep, e.g. $\beta_2 \gtrsim 2$. It is important to note that we have arrived at this conclusion without considering any additional constraints imposed by e.g. the observed high-energy variability. In other words, even if the observed variability is not faster than \sim hour timescale, the cascade emission initiated by photohadronic interactions limits the Doppler factor to values larger than 15-20.

The minimum Doppler factor shown in Fig. 1 can be considered as an absolute lower limit, since it was derived using only the

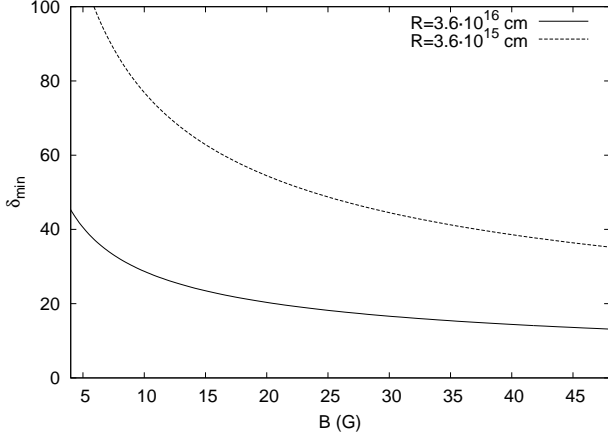


Figure 1. Minimum Doppler factor δ_{\min} as a function of the magnetic field strength for $R = 3.6 \times 10^{16}$ cm (solid line) and $R = 3.6 \times 10^{15}$ cm (dashed line). The region below the curves leads to modification of the proton synchrotron spectrum due to the enhanced cascade emission, and is therefore, forbidden. Other parameters used for the plot are: $\nu_s = \epsilon_s/h = 3.2 \times 10^{13}$ Hz, $L_s = 6.3 \times 10^{45}$ erg/s, $\nu_\gamma = 10^{22}$ Hz, $\eta = 0.2$, $p = 2.3$, $\beta_1 = 0.7$ and $\beta_2 = 1.35$.

internally produced radiation. If we were to include an extra low-energy photon component in our calculations, such as the BLR photon field, the Doppler factor would have to be larger than δ_{\min} (see Sect. 4).

3 NUMERICAL APPROACH

In what follows we will expand upon the idea presented in the previous section by including in our calculations the emission from the BLR. Our working framework is analogous to that adopted in the previous section but with two main differences:

(i) the use of the numerical code described in Dimitrakoudis et al. (2012) allows us to make no assumptions about the photohadronic emission and the initiated EM cascade. The steady-state proton, electron and photon distributions are self-consistently calculated by numerically solving the system of coupled integrodifferential equations that describes their evolution in the energy- and time-phase space.

(ii) the minimum Doppler factor for a particular FSRQ will be derived by fitting its multi-wavelength contemporaneous observations with the proton synchrotron model.

3.1 Model

We model the blazar emission region as a spherical homogeneous blob of radius R that contains a tangled magnetic field of strength B . The region moves with a bulk Lorentz factor Γ at a small angle θ_{obs} with respect to the observer. The respective Doppler factor δ is defined as $\delta = \Gamma^{-1}(1 - \beta \cos \theta_{\text{obs}})^{-1}$. We assume that relativistic electrons and protons with power-law distributions are being injected into the source at a constant rate, while they may physically escape at an energy-independent timescale that is set equal to the crossing time $t_{\text{cr}} = R/c$ of the emission region. Electrons lose energy through synchrotron radiation and inverse Compton scattering on the external photons (EC) as well as on the internally produced synchrotron

photons (SSC). Protons lose energy by emitting synchrotron radiation and through the photohadronic channels of Bethe-Heitler pair production and photopion production (e.g. Dimitrakoudis et al. 2012). The loss processes will lead to the injection of secondary electrons and photons which are, respectively, subjected to synchrotron/inverse Compton scattering and photon-photon absorption. We refer the reader to Dimitrakoudis et al. (2014) for a detailed description of the physical processes.

As already mentioned in the introduction, our working hypothesis is that the low- and high-energy components of the blazar SED are the result of primary electron and proton synchrotron radiation, respectively (see e.g. Mücke & Protheroe 2001). The emission produced through photohadronic interactions appears at even higher energies than the high-energy component, and is subjected to photon-photon absorption.

We assume that the spectrum of the external ultraviolet (UV) radiation arises from an optically thick accretion disk, and is then scattered by the BLR clouds. For simplicity, we approximate the accretion disk emission with a black-body spectrum⁴ that peaks at the observed energy. For the BLR we adopt the geometry presented in Nalewajko et al. (2014)⁵, and illustrated in Fig. 2. The inner radius of the BLR is defined as R_{BLR} , which is related to the accretion disk luminosity L_{ad} (Ghisellini & Tavecchio 2008) as

$$R_{\text{BLR}} \approx 10^{17} \text{ cm } L_{\text{ad},45}^{1/2}. \quad (35)$$

Other sources of external photons could be the reprocessed line emission or infrared radiation from a dusty torus. In what follows, we will not include in our calculations the radiation from the torus, since its luminosity and size are less well-defined than those for the BLR. We will also neglect the direct irradiation from the accretion disk (Dermer & Schlickeiser 2002). This is a safe assumption as long as the emission region lies at (e.g. Ghisellini & Madau 1996; Sikora et al. 2009)

$$r > 0.8 \left(\frac{R_g R_{\text{BLR}}^2}{\xi_{\text{BLR}}} \right)^{1/3} \approx 0.01 \text{ pc } \xi_{\text{BLR},-1}^{-1/3} L_{\text{ad},45}^{1/3} M_{\text{BH},9}^{1/3}, \quad (36)$$

where M_{BH} is the black hole mass, which for 3C 273 is $M_{\text{BH},9} \equiv M_{\text{BH}}/(10^9 M_\odot) \approx 0.9 - 2.4$ (Peterson et al. 2004; Paltani & Türlér 2005), and ξ_{BLR} is a dimensionless factor that incorporates all the details about the geometry and the irradiation of the BLR from the accretion disk. A representative value is $\xi_{\text{BLR}} \sim 0.1$ (Sikora et al. 2009), while values $\lesssim 0.01$ are considered to be very low (e.g. Nalewajko et al. 2014).

The emission region, which is depicted as a yellow blob in Fig. 2, is located at a distance r in the blazar jet. In this study, we treat r as a free parameter, i.e. $r \leq R_{\text{BLR}}$, with the aim of imposing a minimum value on the ratio r/R_{BLR} . As shown in Fig. 2, the radius of the emission region is kept constant, with only the constraint of being smaller than the transverse size of the jet at a distance r , i.e. $R \leq r\theta \leq r/\Gamma$, where we also used $\theta\Gamma \lesssim 1$ (see Nalewajko et al. 2014 and discussion, therein). We will return to this issue in Sect. 5, where we discuss how our results would be altered, if we allowed $R \propto r^s$. In principle, R is related to the observed variability timescale as $t_{\text{var}} \gtrsim (1+z)R/c\delta$. As t_{var} may

⁴ An optically thick, geometrically thin disk, i.e. a Shakura-Sunyaev disk, is better described by a multi-temperature black body, whose flux scales as $F(\epsilon) \propto \epsilon^{1/3} \exp(-\epsilon/\epsilon_0)$. However, the details of the accretion disk spectrum do not affect our analysis.

⁵ Some observations may suggest, however, a planar geometry for certain FSRQs (e.g. Stern & Poutanen 2014).

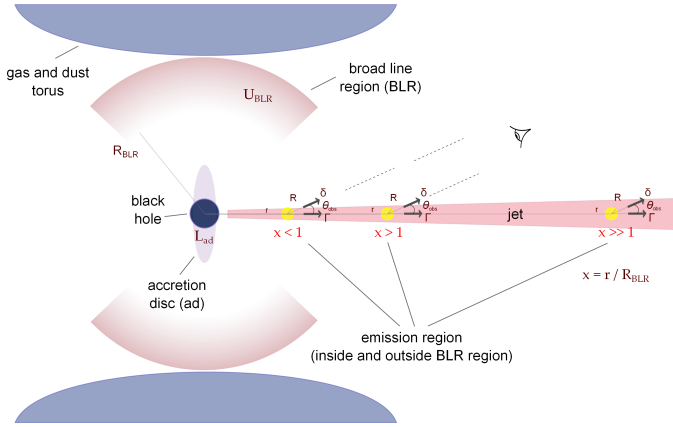


Figure 2. Sketch of the geometry of the emission region and its surrounding sources of radiation, for an FSRQ.

take a wide range of values, even for the same source, depending on the observing period and energy band (for 3C 273 see e.g. Kataoka et al. 2002; Soldi et al. 2008), we choose to use R instead of t_{var} as the free parameter. We discuss the variability constraints later in Sect. 4.3.

Following Sikora et al. (2009) and Nalewajko et al. (2014), we write the energy density of the BLR region as measured in the rest frame of the emission region as

$$u'_{\text{BLR}} = \frac{0.4\xi_{\text{BLR}}\Gamma^2 L_{\text{ad}}}{3\pi c R_{\text{BLR}}^2} \lambda(x), \quad (37)$$

where the function λ is defined as

$$\lambda(x) = \frac{1}{1 + x^4}, \quad (38)$$

and $x \equiv r/R_{\text{BLR}}$. Similarly, the BLR photon energy as measured in the comoving frame of the emission region is given by (Nalewajko et al. 2014)

$$\epsilon'_{\text{BLR}} \simeq \Gamma \epsilon_{\text{BLR}} \frac{1}{1 + x^3}. \quad (39)$$

An important quantity in our analysis is the so-called photon compactness⁶, which is defined as $\ell_\gamma \equiv u'_\gamma \sigma_T R / m_e c^2$, where u'_γ is the co-moving energy density of an arbitrary photon field. Using eq. (37) we may write the BLR photon compactness as

$$\ell_{\text{BLR}} = \ell_0 \Gamma^2 \lambda(x), \quad (40)$$

where

$$\ell_0 = \frac{0.4\xi_{\text{BLR}}\sigma_T R L_{\text{ad}}}{3\pi m_e c^3 R_{\text{BLR}}^2}. \quad (41)$$

Thus, the total photon compactness in the emission region, which is relevant to the calculations of photohadronic emission, is given by $\ell_{\text{tot}} = \ell_{\text{BLR}} + \ell_{\text{syn}}$, where ℓ_{syn} is the compactness of internally produced synchrotron photons. We note that we do not take into account the anisotropy of the BLR photon field as seen in the emission region in the calculations of photopion production (see also, Atoyan & Dermer 2001; Tavecchio et al. 2014).

⁶ Similarly, we have used in Sect. 2 the term proton compactness (see eq. (27)).

3.2 Method

The algorithm we follow in our numerical approach is described below.

3.2.1 No external radiation

We start by assuming that ℓ_{BLR} is negligible with respect to the compactness of the internally produced photons, namely $\ell_{\text{BLR}} \ll \ell_{\text{syn}}$. This can be seen as the case of minimal compactness. For a given pair of B and R we

- (i) choose a high value for the Doppler factor δ , e.g. 50;
- (ii) choose values for the rest of the parameters, e.g. $\ell_{\text{p,e}}$ and $\gamma_{\text{p,max}}$, that lead to a reasonable fit of the SED. This is defined by the curve that passes within the error bars of most of the observational points, with particular emphasis on the highest energy ones, that are more directly affected by secondary particles from photohadronic processes within this model. We are not interested in the absolute best fit, as would be determined by a χ^2 test, but rather a good enough one, as determined visually;
- (iii) if the derived photon spectrum describes the SED reasonably well, we return to step (i) and choose a smaller value of δ ; if the photon spectrum does not fit the SED for the adopted Doppler factor because of enhanced photohadronic emission, we stop and define the current value of the Doppler factor as δ_{min} .

3.2.2 Internal and external radiation

As a second step, we include the BLR emission into the calculation of the broad-band photon spectrum. For each value of $\delta \approx \Gamma$, we obtain the multi-wavelength spectra for different values of ℓ_{BLR} . Each pair of $(\delta, \ell_{\text{BLR}})$ translates into a pair of (δ, x) through eq. (40). Thus, numerical runs for fixed δ and ℓ_{BLR} imply different locations of the emission region in the jet, i.e.

$$x = \left(\frac{\ell_0}{\ell_{\text{BLR}}} \delta^2 - 1 \right)^{1/4}. \quad (42)$$

This corresponds also to different comoving photon energies ϵ'_{BLR} (see eq. (39)). It is important to note that the inclusion of the BLR radiation does not affect the values of $\ell_{\text{e,p}}$ and $\gamma_{\text{p,max}}$ that we derived previously (Sect. 3.2.1), since the SED is fitted by the synchrotron radiation of primary electrons and protons. This shows the secondary role of the external radiation in the proton synchrotron model, in contrast to the EC leptonic models.

We then determine that value of ℓ_{BLR} above which the cascade emission modifies the proton synchrotron radiation spectrum at a few GeV in a way that the total emission exceeds the observations. As can be evidenced by eq. (42), the maximum value of the BLR compactness translates into a lower limit of r/R_{BLR} . This parametrization of the problem allows, therefore, for solutions within or outside the BLR and is a generalization of the approach presented in Sect. 3.2.1. We note that the cascade emission depends on both ℓ_{BLR} and ϵ'_{BLR} , which affect the photohadronic production rates in a direct and indirect way, respectively. The value of ϵ'_{BLR} affects the energy thresholds for photohadronic interactions. Thus, for a given Doppler factor, a choice of a higher value of ℓ_{BLR} does not necessarily mean that the luminosity of the cascade emission will be higher.

4 RESULTS: APPLICATION TO 3C 273

We apply our method to the well-known FSRQ 3C 273 at redshift $z = 0.158$. The optical-UV spectrum of 3C 273 shows a prominent excess of emission, which is mainly interpreted as a contribution of the accretion disk emission (see Ulrich, 1981; Soldi et al., 2008, and references therein). The detection of lines in the optical-UV spectrum of 3C 273, e.g. Ly- α , CIV, OVI, CIII, NIII, and SVI (e.g. Paltani & Türlér 2003, and references therein) is connected with the BLR. The accretion disk and BLR luminosities of 3C 273 are well-defined, i.e. $L_{\text{ad}} = 1.3 \times 10^{47}$ erg/s (Vasudevan & Fabian 2009) and $L_{\text{BLR}} = 9.1 \times 10^{45}$ erg/s (Peterson et al. 2004). The knowledge of both L_{ad} and L_{BLR} reduces the number of free parameters entering in the model (see also Böttcher et al. 2013). Other parameters describing the BLR are $R_{\text{BLR}} \approx 1.1 \times 10^{18}$ cm (from eq. (35)), $\epsilon_{\text{BLR}} = 8$ eV and $\xi_{\text{BLR}} = 0.1$. As can be evidenced by the ASI Science Data Centre (ASDC)⁷, there is a huge amount of archival and non-simultaneous observations for 3C 273. As simultaneous multi-wavelength observations are important for our analysis, we use the dataset by Abdo et al. (2010). We emphasize, though, that our method can be easily applied to different broad-band simultaneous data, since it is based on a generic idea.

4.1 No external radiation or $r \gg R_{\text{BLR}}$

Figure 3 demonstrates the effect of the cascade emission on the high-energy part of the spectrum as the Doppler factor of the emission region progressively decreases, in the minimal scenario where only internal radiation is a target for photohadronic interactions. The three panels (from top to bottom) correspond to different magnetic field strengths, namely $B=30$ G, 15 G and 7.5 G. The radius of the emission region is assumed to be $R = 3.6 \times 10^{16}$ cm in all runs. For a fiducial value of $\delta = 15$, our choice results in $t_{\text{var}} \sim 1$ day, which is typical for 3C 273 (Courvoisier et al. 1988). Other parameters used and kept fixed in the numerical runs are: $\gamma_{e,\text{min}} = 1.6 \times 10^2$, $\gamma_{p,\text{min}} = 1$, $\gamma_{e,\text{max}} = 5 \times 10^3$, $p_e = 2.7$ and $p = 2.3$; both distributions of primary particles were modelled as $n_i \propto \gamma^{-p_i} e^{-\gamma/\gamma_{i,\text{max}}}$, $i = e, p$. The parameters that had to be adjusted in order to model the SED for the different Doppler factor values are listed in Table 1. In all cases, the plateau-like emission above a few GeV ($> 10^{24}$ Hz) is the result of the EM cascade initiated by VHE γ -rays produced in photohadronic interactions. Spectra shown with red thick lines correspond to the minimum value of the Doppler factor that can explain the simultaneous SED. For $\delta < \delta_{\text{min}}$, the photon spectra above $> 10^{24}$ Hz exceed the observations.

At this point, it is interesting to compare the numerically derived ℓ_p and δ_{min} listed in Table 1 with the respective values predicted by our analysis in Sect. 2. This is exemplified in Fig. 4 where the top and bottom panels show the comparison for ℓ_p and δ_{min} , respectively. In both panels, the values from the numerical analysis are shown with symbols, while the curves are calculated using eq. (27) for $R = 3.6 \times 10^{16}$ cm, $\gamma_\gamma = 10^{22}$ Hz, $L_\gamma = 6.3 \times 10^{46}$ erg/s and $p = 2.3$ (top panel) and eq. (32) for $\nu_s = \epsilon_s/h = 3.2 \times 10^{13}$ Hz, $L_s = 6.3 \times 10^{45}$ erg/s, $\nu_\gamma = 10^{22}$ Hz, $\eta = 0.2$, $p = 2.3$, $\beta_1 = 0.7$, and $\beta_2 = 1.35$ (bottom panel).

In both panels, our analytical curves are in good agreement with the numerical values determined through the SED modelling, with some deviation becoming systematically larger for $B = 7.5$ G (top panel) and $R = 3.6 \times 10^{15}$ cm (bottom panel). However, it is

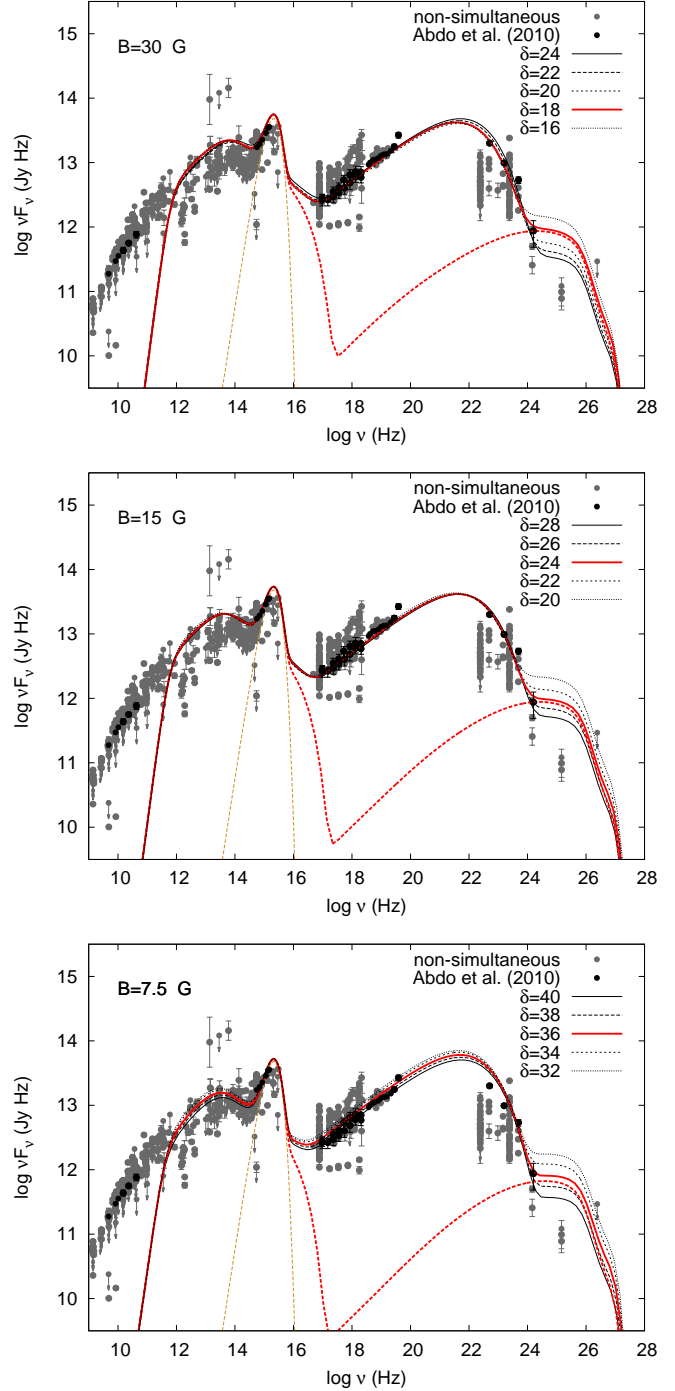


Figure 3. Proton synchrotron model fits to the simultaneous multi-wavelength data of 3C 273 by Abdo et al. 2010 (black symbols) for $B=30$ G, 15 G and 7.5 G (top to bottom), in the limiting case of $\ell_{\text{BLR}} \ll \ell_{\text{syn}}$ or, equivalently $r \gg R_{\text{BLR}}$. In each panel, the SED is modelled using different values of the Doppler factor. Spectra shown with red lines correspond to the minimum value of the Doppler factor that can explain the simultaneous SED. The respective spectrum when proton synchrotron radiation is omitted, which reveals the underlying spectrum of the EM cascade, is shown with a red dashed line. The accretion disk spectrum is overplotted with an orange dashed line. Grey symbols are non-simultaneous and archival observations taken from ASDC.

⁷ <http://www.asdc.asi.it/SED>

Table 1. Parameter values used for modelling the multi-wavelength emission of 3C 273, as illustrated in Fig. 3. Not all cases listed in this Table are depicted in Fig. 3, but we include them for completeness reasons. Other parameters used are kept fixed (see text).

	δ	ℓ_e (in log)	ℓ_p (in log)
B=30 G			
$\gamma_{p,max} = 10^8$			
	28	-5.2	-3.5
	26	-5.1	-3.4
	24	-4.9	-3.2
	22	-4.8	-3.1
	20	-4.6	-3.0
(δ_{min})	18	-4.4	-2.8
	16	-4.2	-2.6
B=15 G			
$\gamma_{p,max} = 1.2 \times 10^8$			
	32	-5.5	-3.3
	30	-5.3	-3.1
	28	-5.2	-3.0
	26	-5.1	-2.9
(δ_{min})	24	-4.9	-2.7
	22	-4.8	-2.6
	20	-4.6	-2.4
B=7.5 G			
$\gamma_{p,max} = 1.6 \times 10^8$			
	40	-6.0	-3.0
	38	-5.9	-2.9
(δ_{min})	36	-5.7	-2.7
	34	-5.6	-2.6
	32	-5.5	-2.5

remarkable how well the analytical curves follow the trend found numerically, and especially for δ_{min} , since we made several approximations in order to derive an analytical expression (eq. 32). A quantitative difference between the curves is something to be expected, since the numerical analysis: (i) takes into account the emission from secondary pairs (from Bethe - Heitler and π^+ decays) in the formation of the EM cascade, (ii) makes no assumptions about the photohadronic production rates, and (iii) takes into account the spectral shape of the EM cascade.

For completeness reasons, we repeated the modelling procedure for a smaller emission region having $R = 3.6 \times 10^{15}$ cm. The bottom panel of Fig. 4 shows that unreasonably high values of the Doppler factor ($\delta \gtrsim 40$) are required, in this case, to avoid the effects of the EM cascade, while only very strong magnetic fields ($B \gg 50$ G), can bring the Doppler factor to lower values.

4.2 Internal and external radiation

Following the method described in Sect. 3.2.2, we derived the minimum value of the ratio r/R_{BLR} for the three cases considered previously. Our results are summarized in Table 2 and Fig. 5. The different curves are obtained for $B = 30$ G, 15 G and 7.5 G. The results obtained from the numerical fitting are shown as symbols, while the curves are the result of interpolation. Only the region above each curve is allowed, as values below the curve lead to significant emission from the EM cascade. Thus, each curve is the locus of points corresponding to the minimum distance, r_{min} , for

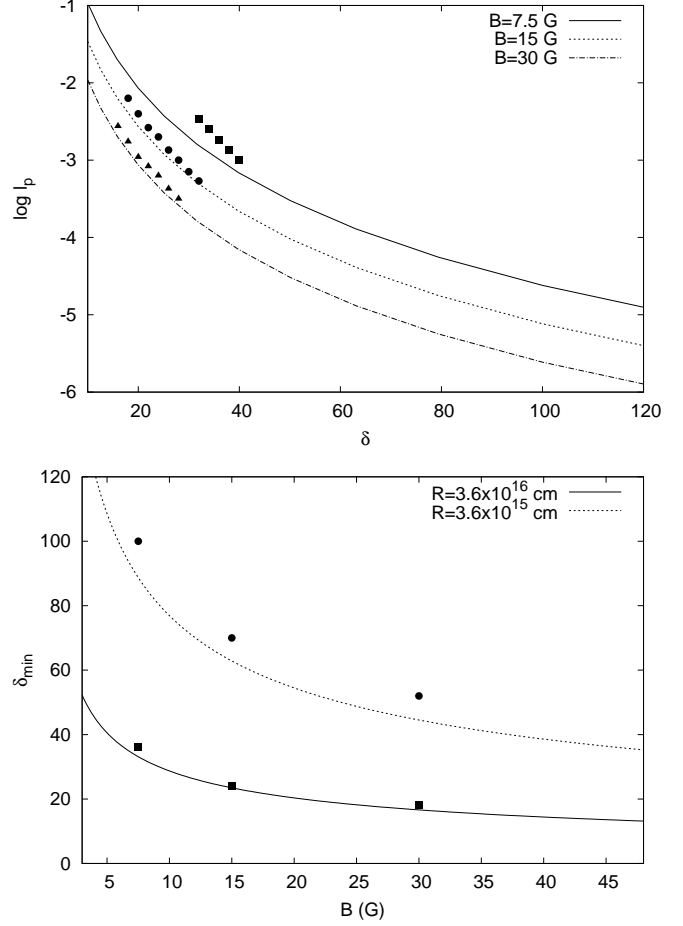


Figure 4. Comparison between the analytical (curves) and numerical (symbols) results. Top panel: ℓ_p as a function of δ for $B = 7.5$ G (solid line/squares), 15 G (dotted line/circles) and 30 G (dashed-dotted line/triangles). Bottom panel: δ_{min} as a function of B (bottom panel) for $R = 3.6 \times 10^{16}$ cm (solid line/squares) and $R = 3.6 \times 10^{15}$ cm (dotted line/circles).

various Doppler factor values. The curves can be also safely extrapolated to higher Doppler factor values, since a power-law dependence is established, namely $r_{min}/R_{BLR} \propto \delta^{1/2}$. The abrupt increase of r_{min}/R_{BLR} occurs at $\delta = \delta_{min}$, as expected. We remind that δ_{min} is derived in the limiting case of $\ell_{BLR} \ll \ell_{syn}$ or, equivalently, $r \gg R_{BLR}$.

Figure 5 reveals the following trend: curves move from the lower left part to the upper right part of the plot for progressively weaker magnetic fields. The horizontal shifting of the curves can be easily understood by inspection of eq. (32), which shows that $\delta_{min} \propto B^{-(3+\beta_2)/(p+3+3\beta_2)}$. For a given δ , weaker magnetic fields require higher values of the proton compactness to explain the observed γ -ray luminosity, which in turn enhances the EM cascade emission. To avoid an excess in γ -rays due to the cascade emission, the emission region should be located even further out. This qualitatively explains the vertical shift of the curves in Fig. 5.

Figure 5 shows that the emission region of 3C 273 in the proton synchrotron scenario cannot be located in the BLR region, at least for $B \leq 30$ G and $R = 3.6 \times 10^{16}$ cm. Let us discuss how a different choice of R and B would affect our conclusion. A choice of a smaller radius, e.g. $R \sim 10^{15}$ cm, would have a similar effect on the curves as that of a decreasing magnetic field (shifting to the

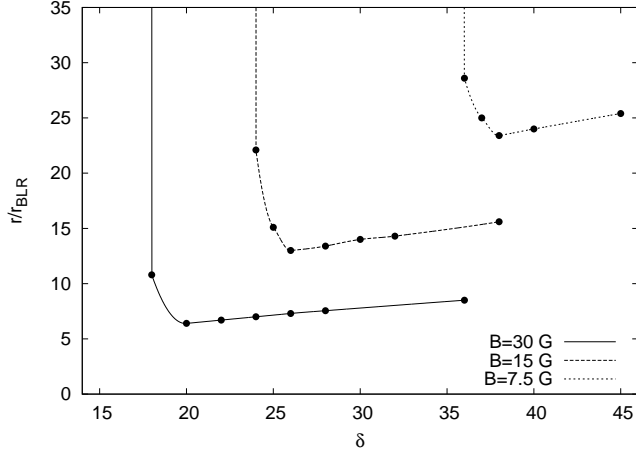


Figure 5. Plot of the ratio r/R_{BLR} as a function of the Doppler factor for three values of the magnetic field marked on the plot and $R = 3.6 \times 10^{16}$ cm. Symbols and lines are used for displaying the numerical results and the interpolated values, respectively. Only the region above each curve is allowed, as values below the curve lead to significant emission from the EM cascade. The abrupt increase of r/R_{BLR} occurs at $\delta = \delta_{\text{min}}$ defined by eq. (32).

Table 2. Maximum ℓ_{BLR} and, equivalently, minimum r/R_{BLR} as determined by modelling of the multi-wavelength emission of 3C 273 for a given Doppler factor and magnetic field strength. The method for the determination or their values is described in Sect. 3.2.2. All other parameters are same as in Table 1.

δ	ℓ_{BLR}	r/R_{BLR}
B=30 G		
28	10^{-4}	7.5
26	10^{-4}	7.3
24	10^{-4}	7.0
22	10^{-4}	6.7
20	10^{-4}	6.4
18	10^{-5}	10.8
B=15 G		
38	10^{-5}	15.6
32	10^{-5}	14.3
30	10^{-5}	13.9
28	10^{-5}	13.4
26	10^{-5}	12.9
25	5×10^{-6}	15.1
24	10^{-6}	22.1
B=7.5 G		
45	2×10^{-6}	25.4
40	2×10^{-6}	24.0
38	2×10^{-6}	23.4
37	10^{-6}	27.4
36	8×10^{-7}	28.6

upper right part of Fig. 5). Only if the emission region were larger and, thus, less compact could it be located within the BLR. However, as we show in Sect. 4.3, this scenario becomes less plausible when the variability of the source is taken into account. In addition, the jet power of a larger emission region would significantly exceed the accretion power of 3C 273 (see details in Sect. 4.3).

In principle, the emission region could be located within the

BLR for sufficiently large magnetic fields, namely $B \gg 30$ G, according to the trend we find in Fig. 5. The question that arises in this case is whether the required B values are plausible or not. Instead of performing additional simulations, we can address the question with the analytical tools presented in Sect. 2. Inspection of Tables 1 and 2, shows that at the minimum distance r_{min} the electron and BLR compactnesses are approximately equal, while $\delta = \delta_{\text{min}} + \epsilon$, with $\epsilon \simeq 1 - 2$. Since the electron compactness is a good proxy for the internal synchrotron photon compactness, we can estimate the minimum distance by requiring $\ell_{\text{BLR}}(\delta_{\text{min}}) \simeq \ell_{\text{syn}}(\delta_{\text{min}})$ or, equivalently

$$\frac{\delta_{\text{min}}^2 \ell_0}{1 + x_{\text{min}}^4} \simeq \frac{\sigma_{\text{T}} L_{\text{syn}}}{4\pi R m_e c^3 \delta_{\text{min}}^4}, \quad (43)$$

where δ_{min} is given by eq. (32). For $R = 3.6 \times 10^{16}$ cm and for all other parameters same as in Fig. 1, we find that $r_{\text{min}}/R_{\text{BLR}} < 1$ for $B \gtrsim 450$ G. We can therefore argue that the emission region of 3C 273 cannot be located within the BLR for plausible parameter values.

4.3 Additional constraints

The constraints on the Doppler factor and on the distance of the emission region from the super-massive black hole were derived based only on the photohadronic emission and the initiated EM cascade. These can become even more tight when combined with information about the variability of the source and the energetics of the emission region.

4.3.1 Variability

The observed high-energy variability in blazars may range from hours up to few days depending on the flaring activity. For example, the shortest variability timescales probed by FERMI-LAT are several hours (Tavecchio et al. 2010; Foschini et al. 2011; Saito et al. 2013). In order to keep our analysis as generic as possible, we chose R and δ to be independent parameters. Here, we revise our previous results by including the variability information. If t_{var} is the observed variability timescale, δ and R should satisfy the causality condition

$$\delta \geq \delta_{\text{var}} \equiv \frac{R(1+z)}{ct_{\text{var}}}. \quad (44)$$

Figure 6 illustrates the revised parameter space $\delta - B$ for $R = 3.6 \times 10^{16}$ cm and three indicative values of the observed variability timescale marked on the plot. The regions that lie above the horizontal dotted and solid lines denote areas where both the EM cascade and variability constraints are satisfied. For $t_{\text{var}} = 1$ d, the variability offers no additional constraint over δ_{min} . However, for $t_{\text{var}} \lesssim 12$ h the lower limit δ_{var} becomes more constraining than the lower limit derived imposed by the EM cascade.

Similarly, the $r/R_{\text{BLR}} - \delta$ parameter space can be further constrained by including the variability constraint. This is illustrated in Fig. 7. The vertical lines show δ_{var} calculated using eq. (44) for $R = 3.6 \times 10^{16}$ cm and three indicative values of t_{var} (from left to right, $t_{\text{var}} = 24$ h, 12 h and 6 h). To the right of those vertical lines are regions where the causality condition is satisfied. The EM cascade does not exceed the γ -ray observations at a few GeV for parameters drawn above the curves. Finally, the coloured regions denote the parameter space where both requirements are satisfied.

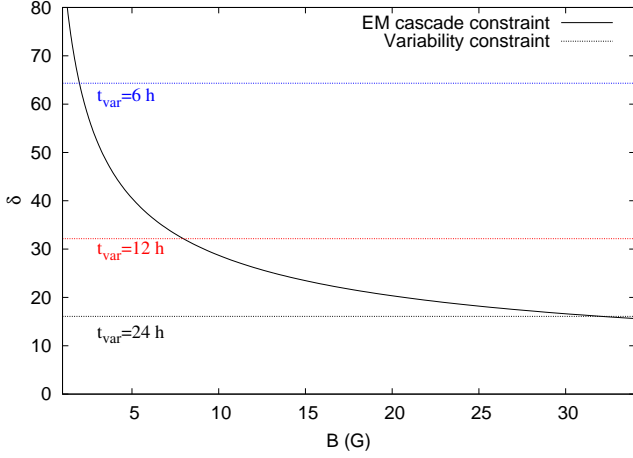


Figure 6. Same as Fig. 1 with the addition of the variability constraint $\delta \geq \delta_{\text{var}}$ (dotted lines) for $R = 3.6 \times 10^{16}$ cm and three indicative values of t_{var} marked on the plot. The curves of δ_{min} are calculated using eq. (32). Only the regions that lie above the horizontal dotted lines, satisfy the variability constraint. All other parameters are same as in Fig. 1.

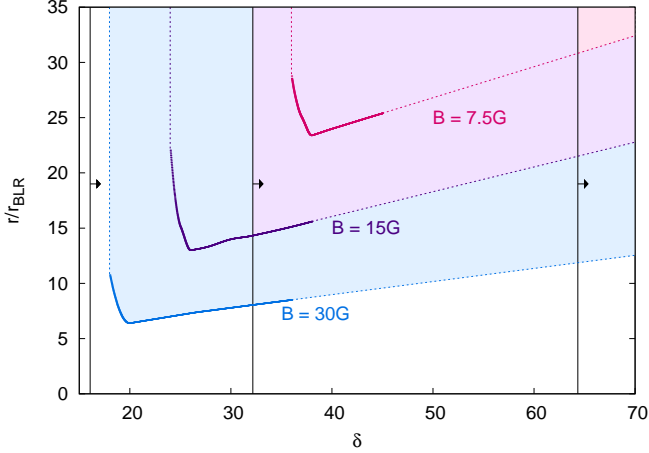


Figure 7. The revised parameter space $r/R_{\text{BLR}} - \delta$ for 3C 273 after taking into account the variability constraint $\delta \geq \delta_{\text{var}}$ for $R = 3.6 \times 10^{16}$ cm and three values of the magnetic field marked on the plot. Vertical lines denote δ_{var} given by eq. (44). From left to right: $t_{\text{var}} = 24$ h, 12 h and 6 h. The coloured regions above the curves and on the right of the vertical lines denote areas where both the variability and EM cascade constraints are satisfied. All other parameters are same as in Fig. 1.

We find that for \sim day timescale variability the location of the emitting region and the Doppler factor are only limited by the EM cascade. A shorter variability timescale, which has been observed during bright γ -ray flares of 3C 273 (e.g. Rani et al. 2013), can impose tighter constraints on the minimum r and δ ; e.g., for $t_{\text{var}} = 6$ h and $B = 7.5$ G only the upper right corner of the parameter space is allowed.

4.3.2 Jet power

In FSRQs the accretion disk luminosity can be estimated using the BLR luminosity, and the accretion power ($P_{\text{acc}} = \dot{M}c^2$) can be then

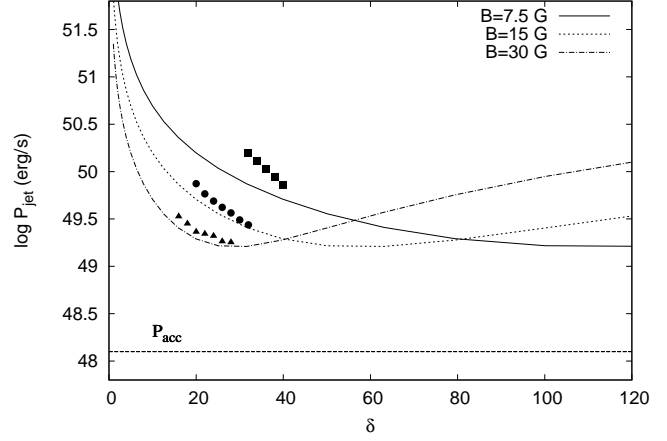


Figure 8. Jet power, as derived in the proton synchrotron model for 3C 273. The values derived by numerically modelling the SED of 3C 273 (see Table 3) are shown as symbols, while the curves are calculated using eq. (48) for $B = 7.5$ G (solid line/squares), 15 G (dotted line/circles) and 30 G (dashed-dotted line/triangles). The horizontal dashed line marks the accretion luminosity given by eq. (45).

calculated as (e.g. Ghisellini et al. 2014)

$$P_{\text{acc}} = 10 \frac{L_{\text{ad}}}{\epsilon_r - 1}, \quad (45)$$

where ϵ_r is the radiative efficiency. In general, the jet power is written as $P_{\text{jet}} = \epsilon_j P_{\text{acc}}$, with $\epsilon_j \lesssim 1.5$ (Zdziarski & Böttcher 2015, and references therein). Although the jet power can exceed the accretion one (e.g. Tchekhovskoy et al. 2011) due to the efficient extraction of energy from a Kerr black hole (Blandford & Znajek 1977), here we consider the more conservative case of $\epsilon_j = 1$. We therefore impose the following ‘energetic’ constraint

$$P_{\text{jet}} \leq P_{\text{acc}}, \quad (46)$$

Neglecting the cold proton and radiation energy densities, the power of a two-sided jet can be written as (e.g. Ghisellini et al. 2014)

$$P_{\text{jet}} \approx 2\pi R^2 \Gamma^2 c (u'_e + u'_p + u'_B) \quad (47)$$

where u'_i ($i = e, p, B$) is the energy density as measured in the rest frame of the emission region. Dropping the electron term (see also Table 3) and using eq. (27) with $\delta \approx \Gamma$, we write the jet power as

$$P_{\text{jet}} \approx \frac{R^2 c}{4} [A (B\delta)^{-(p+1)/2} + (B\delta)^2], \quad (48)$$

where

$$A = \frac{6C_p m_p c^2 L_\gamma}{f_p R^3 \nu_\gamma^{(3-p)/2}}. \quad (49)$$

The jet power given by eq. (48) for $R = 3.6 \times 10^{16}$ cm, $L_\gamma = 6.3 \times 10^{46}$ erg/s, $\nu_\gamma = 10^{22}$ Hz, $p = 2$, and three values of the magnetic field, i.e. $B = 7.5, 15$ and 30 G, is plotted as a function of δ in Fig. 8. Overplotted with symbols are the values calculated using eq. (48) for u'_p determined by the numerical SED modelling of 3C 273 (see also Table 3). Apart from an offset ($\lesssim 3$) between the analytical curve and the numerical values for the case of $B = 7.5$ G (see also Fig. 4), the two results are in good agreement. Figure 8 shows that in all our SED fits the jet power is dominated by the energy density of relativistic protons, i.e. $P_{\text{jet}} \propto (B\delta)^{-(p+1)/2}$, while it exceeds $P_{\text{acc}} = 1.3 \times 10^{48}$ erg/s (dashed line). Even the minimum jet

Table 3. Energy densities of relativistic electrons and protons (in the co-moving frame) as determined by modelling of the multi-wavelength emission of 3C 273 for a given Doppler factor and magnetic field strength. The jet power is listed in the last column of the table. All other parameters are same as in Table 1.

	δ	$u'_e{}^a$	$u'_p{}^b$	$P_{\text{jet}}{}^c$
B=30 G ($u'_B = 35.8 \text{ erg/cm}^3$)				
	28	1.7	58	1.8
	26	2.3	75	1.8
	24	3.3	113	2.1
	22	4.4	150	2.2
	20	6.5	200	2.3
	18	11.0	320	2.8
	16	16.8	502	3.3
B=15 G ($u'_B = 9 \text{ erg/cm}^3$)				
	32	2.8	100	2.7
	30	3.8	132	3.1
	28	5.1	182	3.7
	26	6.8	245	4.2
	24	9.6	339	4.9
	22	13.7	483	5.8
	20	20.5	753	7.4
B=7.5 G ($u'_B = 2.2 \text{ erg/cm}^3$)				
	40	2.2	182	7.2
	38	3.0	244	8.7
	36	4.1	332	10.6
	34	5.5	458	13.0
	32	7.5	621	15.6

^a Electron energy density in units of 10^{-5} erg/cm^3 .

^c Electron energy density in erg/cm^3 .

^b Jet power in units of 10^{49} erg/s .

power ($P_{\text{jet,min}}$) exceeds the accretion power by approximately one order of magnitude (see also Zdziarski & Böttcher 2015). Thus, at least for the particular choice of R and B , relation (46) cannot be satisfied, and in this regard, it cannot further constrain the parameter space.

The relatively good agreement between the analytical and numerical results for the jet power allows us to use expression (48) for investigating the dependence of $P_{\text{jet,min}}$ on the parameters, and to search for those, if any, that can bring the jet power closer to the accretion luminosity. The jet power given by eq. (48) is minimized for

$$\delta_0 B_0 = \left(A \frac{p+1}{4} \right)^{2/(p+5)} \quad (50)$$

and its minimum value for a given source (L_γ , ν_γ and p , fixed) depends only the radius R through

$$P_{\text{jet,min}} = \tilde{A} R^{(2p-2)/(p+5)}, \quad (51)$$

where

$$\tilde{A} = \frac{c}{4} \left(\frac{6C_p m_p c^2 L_\gamma}{f_p \nu_\gamma^{(3-p)/2}} \right)^{4/(p+5)} \left(s^{-(p+1)/(p+5)} + s^{4/(p+5)} \right) \quad (52)$$

and

$$s = \frac{p+1}{4}. \quad (53)$$

The requirement $P_{\text{jet,min}} = P_{\text{acc}}$ is satisfied for

$$R_0 = \left(\frac{P_{\text{acc}}}{\tilde{A}} \right)^{(p+5)/(2p-2)} \quad (54)$$

which for 3C 273 and $p = 2.3$ becomes $R_0 \sim 10^{14} \text{ cm}$. Substitution of R_0 into eq. (50) results in $\delta_0 B_0 \sim 5 \times 10^4$ (in cgs units), namely the Doppler factor and the magnetic field should take extreme values.

Summarizing, we showed explicitly that in the proton synchrotron scenario for the multi-wavelength emission of 3C 273 there are no reasonable physical parameters that can bring the jet power close the accretion power. In all cases, we find $P_{\text{jet}} \gtrsim 10 P_{\text{acc}}$, in agreement with the independent analysis by Zdziarski & Böttcher (2015).

5 DISCUSSION

The derivation of constraints for the Doppler factor and/or the location of the emission region in the leptonic framework of blazar emission has been the subject of several studies (e.g. Dondi & Ghisellini 1995; Poutanen & Stern 2010; Tavecchio et al. 2010; Dotson et al. 2012; Cerruti et al. 2013; Dermer et al. 2014; Nalewajko et al. 2014; Zacharias 2015). The exploration of such constraints within the confines of alternative models is a method that may lead to their eventual verification or exclusion, with new observations potentially reshaping the available parameter space. In this study, we expand this search by adopting the proton synchrotron model for the γ -ray blazar emission.

Under the assumption that the high-energy component of the SED in FSRQs is explained in terms of proton synchrotron radiation, we showed that for low enough values of the Doppler factor δ , the emission from the EM cascade may exceed the observed $\sim \text{GeV}$ flux. In fact, the superposition of the EM cascade and proton synchrotron components results in a spectral hardening of the total emission above a few GeV (see Fig. 3). From our analysis, it is not clear why the proton synchrotron component should dominate in the hard X-ray/soft γ -ray regime while the EM cascade should be suppressed. One could then naturally pose the following question: *Would it be possible to fit the SED with the cascade component instead of the proton synchrotron component, and would the parameters of such a model be reasonable?* Roughly speaking, the peak of the cascade spectrum can be found by the condition $\tau_{\gamma\gamma}(\epsilon_\star) \approx 1$ (for more details, see Mannheim (1993)). For the parameter values used throughout the text, we showed that $\epsilon_\star \sim 18 \text{ GeV}$ (see eq. 17). In principle, one could find parameter values that could bring ϵ_\star down to a few MeV, since $\epsilon_\star \propto L_s^{-2} R^2 \delta^8 \epsilon_s$. In this scenario, the peak luminosity of the cascade should be higher in order to explain the observed peak γ -ray luminosity, namely $L_{\pi^0 \rightarrow 2\gamma}^{\text{abs}} \simeq \tau_{p\pi} L_p \simeq L_\gamma$. Unless $\tau_{p\pi} \gtrsim 1$, which would correspond to $R \sim 10^{14} \text{ cm}$, $B \lesssim 1 \text{ G}$, and $\delta \lesssim 5$ (see eq. (24)), this scenario would require higher proton luminosities, and therefore, even more extreme jet powers than those listed in Table 3. These estimates, however, are made by considering only the internal synchrotron photons as targets for both photopion interactions and $\gamma\gamma$ absorption. A proper answer to the question posed above requires a self-consistent calculation of the cascade emission by taking into account the external photon fields as targets for both $\gamma\gamma$ and photopion interactions and by focusing on a different parameter regime than the one considered here. Such

an investigation is interesting on its own, and will be the subject of a future study.

A serious challenge to the proton synchrotron model arises from the need for high values of B at distances far from the central black hole. Pushkarev et al. (2012) have determined, using core shift measurements, the magnetic field - distance relation to be $B \sim 0.4 \text{ G} \times (1 \text{ pc}/r)$ (see also Zdziarski et al. 2014, for a theoretical investigation). Savolainen et al. (2008) have presented specifically for 3C 273 magnetic field measurements of its pc-scale inner jet structure. Assuming that the jet's angle to our line of sight is 10° (Stawarz 2004), it would appear that $B \leq 8 \text{ G}$ at $r \approx 1.25 \text{ pc}$. Applying the linear relation between B and r and using $R_{\text{BLR}} = 0.3 \text{ pc}$, we find that for the values of B considered in Fig. 5 and Fig. 7 our derived values of r/R_{BLR} are over a factor of 5 higher than those needed to accommodate such strong magnetic fields. This would imply that, at least for the case of 3C 273, the magnetic field strength required by the proton synchrotron model at the location of the emission region is in conflict with the observations.

In principle, the parameter space used in modelling the SED could be further constrained by requiring that the jet power (P_{jet}) should not exceed the accretion power (P_{acc}) which, for FSRQs like 3C 273, can be safely estimated. We showed, however, that in the proton synchrotron model for 3C 273 the jet power exceeds that of accretion, i.e. $P_{\text{jet}} \geq 10P_{\text{acc}}$, for all reasonable parameter values. We note, however, that this is as much a problem for leptonic models as for hadronic ones (Ghisellini et al. 2014).

A possible caveat of our analysis is our assumption of a constant radius for the emission region, as well as of a constant magnetic field strength. Assuming that the emission region fills the entire cross section of the jet, one could express the size R as a function of distance r from the central black hole, i.e. $R \propto r^s$ with $s > 0$ depending on the specific model of the jet structure (e.g. Ghisellini et al. 1985; Moderski et al. 2003; Potter & Cotter 2013). Similarly, the magnetic field could be written as $B \propto r^q$ with $q < 0$ (e.g. Vlahakis & Königl 2004; Komissarov et al. 2007). Yet, there would remain some arbitrariness regarding the relation between the magnetic field in the jet and in the emission region, as this would depend on the dissipation mechanism (for a discussion, see Sironi et al. 2015), which in turn depends on the distance from the super-massive black hole (e.g. Sikora et al. 2005; Giannios et al. 2009; Nalewajko 2012). In any case, we can qualitatively predict the effects of an increasing size and decreasing magnetic field strength on the results presented so far. On the one hand, a larger R would loosen the EM cascade constraint, while it would push δ_{var} to higher values. This could bring the location of the emission region closer to or inside the BLR, at the cost of even higher jet powers. On the other hand, a decreasing magnetic field would make the EM cascade more stringent, i.e. higher δ_{min} would push the location of the emission region even further away from the BLR. The impact on jet power would depend on the Doppler factor but it would be marginal, as evidenced by eq. (48). In short, an increasing radius would have the opposite effects from those of a decaying magnetic field. Thus, their combined effect would strongly depend on the details of the model, such as q and s .

The question naturally arises whether the method presented here would yield significantly different results when applied to other FSRQs, or to a flaring period of 3C 273. Our results regarding the high jet power are not expected to differ, since this is an intrinsic feature of the proton synchrotron model (e.g. Böttcher et al. 2013). It is not straightforward, however, what the answer would be regarding the location of the emission region in other luminous blazars. The hypothesis that the emission region, in the hadronic

framework for FSRQs, is located at the $\sim \text{pc}$ scale jet, can be easily tested by applying our method to a sample of densely monitored sources, and we plan to do so in a future study.

6 CONCLUSIONS

We have demonstrated a method of constraining the properties of the γ -ray emitting region in FSRQs within the one-zone proton synchrotron model. Even though the high-energy component of the blazar SED is attributed to synchrotron radiation of relativistic protons, the emission from photohadronic processes cannot be avoided. In fact, the EM cascade initiated by the absorption of photons produced via photohadronic interactions may exceed the observed γ -ray flux at $\sim \text{GeV}$ energies, for small enough Doppler factors. For the purposes of our analytical treatment, we focused on the photons from neutral pion decay, while we neglected the synchrotron emission from Bethe-Heitler pairs and those produced through the decay of charged pions. Therefore, the EM cascade results only from photons from neutral pion decay, which interact with the low-energy synchrotron blazar emission. To avoid a significant alteration of the SED in that energy range, a constraint is set on the luminosity from the EM cascade which is translated to a lower limit on the Doppler factor given by eq. (32). Our analytical calculations were performed in the asymptotic limit where the external radiation from the broad line region (BLR) is negligible. In this regard, δ_{min} can be considered as an absolute lower limit.

We then applied our method to a single FSRQ, namely 3C 273, and generalized our analytical method by including the radiation from the BLR, as well as the variability timescale (t_{var}) in our calculations. Because the BLR energy density in the comoving frame of the emission region is highly dependent on the Doppler factor and its distance from the super-massive black hole in the galactic center, we used the EM cascade argument to determine a minimum distance for each Doppler factor value. Finally, for a given source size, t_{var} sets an additional lower limit on the Doppler factor (δ_{var}). With those additional elements, we arrived at the following robust results: (i) the Doppler factor of the emission region should be higher than 18 – 20 for magnetic field strengths $\leq 30 \text{ G}$ and $\sim \text{day}$ timescale variability; (ii) the γ -ray emission region should be located outside the BLR, namely at $r \gtrsim 10R_{\text{BLR}} \sim 3 \text{ pc}$; (iii) shorter variability timescales, e.g. $\lesssim 12 \text{ hr}$, push both the minimum Doppler factor and distance to even higher values; (iv) the magnetic field strength required by the model at pc scale distances is stronger than that inferred from observations; and (v) the jet power exceeds by at least one order of magnitude the FSRQ accretion power. In conclusion, our results disfavour the proton synchrotron model for the FSRQ 3C 273.

ACKNOWLEDGMENTS

We thank the anonymous referee for the insightful comments that helped us clarify subtleties in the manuscript. We also thank Prof. D. Giannios for fruitful discussions and Prof. A. Mastichiadis for comments on the manuscript. MP acknowledges support by NASA through Einstein Postdoctoral Fellowship grant number PF3 140113 awarded by the Chandra X-ray Center, which is operated by the Smithsonian Astrophysical Observatory for NASA under contract NAS8-03060. We acknowledge the use of data from the ASI Science Data Center (ASDC), managed by the Italian Space Agency (ASI).

REFERENCES

- Aartsen M. G. et al., 2014, *Physical Review Letters*, 113, 101101
- Abdo A. A. et al., 2010, *Astrophysical Journal*, 716, 30
- Aharonian F. A., 2000, *New Astron.*, 5, 377
- ANTARES Collaboration et al., 2015, *Astronomy & Astrophysics*, 576, L8
- Atoyan A., Dermer C. D., 2001, *Physical Review Letters*, 87, 221102
- Begelman M. C., Rudak B., Sikora M., 1990, *Astrophysical Journal*, 362, 38
- Beringer J. et al., 2012, *Phys. Rev. D*, 86, 010001
- Blandford R. D., Rees M. J., 1978, *Phys. Scr.*, 17, 265
- Blandford R. D., Znajek R. L., 1977, *Monthly Notices of the Royal Astronomical Society*, 179, 433
- Błażejowski M., Sikora M., Moderski R., Madejski G. M., 2000, *Astrophysical Journal*, 545, 107
- Bloom S. D., Marscher A. P., 1996, *Astrophysical Journal*, 461, 657
- Böttcher M., Reimer A., Sweeney K., Prakash A., 2013, *Astrophysical Journal*, 768, 54
- Cerruti M., Dermer C. D., Lott B., Boisson C., Zech A., 2013, *Astrophysical Journal Letters*, 771, L4
- Chatterjee R., Nalewajko K., Myers A. D., 2013, *Astrophysical Journal Letters*, 771, L25
- Coppi P. S., Blandford R. D., 1990, *Monthly Notices of the Royal Astronomical Society*, 245, 453
- Courvoisier T. J.-L., Robson E. I., Hughes D. H., Blecha A., Bouchet P., Krisciunas K., Schwarz H. E., 1988, *Nature*, 335, 330
- Dermer C. D., Cerruti M., Lott B., Boisson C., Zech A., 2014, *Astrophysical Journal*, 782, 82
- Dermer C. D., Ramirez-Ruiz E., Le T., 2007, *Astrophysical Journal Letters*, 664, L67
- Dermer C. D., Schlickeiser R., 2002, *Astrophysical Journal*, 575, 667
- Dermer C. D., Schlickeiser R., Mastichiadis A., 1992, *Astronomy & Astrophysics*, 256, L27
- Dimitrakoudis S., Mastichiadis A., Protheroe R. J., Reimer A., 2012, *Astronomy & Astrophysics*, 546, A120
- Dimitrakoudis S., Petropoulou M., Mastichiadis A., 2014, *Astroparticle Physics*, 54, 61
- Dondi L., Ghisellini G., 1995, *Monthly Notices of the Royal Astronomical Society*, 273, 583
- Dotson A., Georganopoulos M., Kazanas D., Perlman E. S., 2012, *Astrophysical Journal Letters*, 758, L15
- Foschini L., Ghisellini G., Tavecchio F., Bonnoli G., Stamerra A., 2011, *Astronomy & Astrophysics*, 530, A77
- Fossati G., Maraschi L., Celotti A., Comastri A., Ghisellini G., 1998, *Monthly Notices of the Royal Astronomical Society*, 299, 433
- Ghisellini G., Madau P., 1996, *Monthly Notices of the Royal Astronomical Society*, 280, 67
- Ghisellini G., Maraschi L., Treves A., 1985, *Astronomy & Astrophysics*, 146, 204
- Ghisellini G., Tavecchio F., 2008, *Monthly Notices of the Royal Astronomical Society*, 387, 1669
- Ghisellini G., Tavecchio F., Maraschi L., Celotti A., Sbarrato T., 2014, *Nature*, 515, 376
- Giannios D., Uzdensky D. A., Begelman M. C., 2009, *Monthly Notices of the Royal Astronomical Society*, 395, L29
- Giommi P. et al., 2012, *Astronomy & Astrophysics*, 541, A160
- Halzen F., Zas E., 1997, *Astrophysical Journal*, 488, 669
- IceCube Collaboration, 2013, *Science*, 342
- Kataoka J., Tanihata C., Kawai N., Takahara F., Takahashi T., Edwards P. G., Makino F., 2002, *Monthly Notices of the Royal Astronomical Society*, 336, 932
- Komissarov S. S., Barkov M. V., Vlahakis N., Königl A., 2007, *Monthly Notices of the Royal Astronomical Society*, 380, 51
- Mannheim K., 1993, *Physical Review D*, 48, 2408
- Mannheim K., Biermann P. L., 1992, *Astronomy & Astrophysics*, 253, L21
- Mannheim K., Biermann P. L., Kruells W. M., 1991, *Astronomy & Astrophysics*, 251, 723
- Maraschi L., Ghisellini G., Celotti A., 1992, *Astrophysical Journal Letters*, 397, L5
- Marscher A. P., Jorstad S. G., Agudo I., MacDonald N. R., Scott T. L., 2012, *ArXiv e-prints*
- Mastichiadis A., Kirk J. G., 1997, *Astronomy & Astrophysics*, 320, 19
- Moderski R., Sikora M., Błażejowski M., 2003, *Astronomy & Astrophysics*, 406, 855
- Mücke A., Engel R., Rachen J. P., Protheroe R. J., Stanev T., 2000, *Computer Physics Communications*, 124, 290
- Mücke A., Protheroe R. J., 2001, *Astroparticle Physics*, 15, 121
- Murase K., Inoue Y., Dermer C. D., 2014, *ArXiv e-prints*
- Nalewajko K., 2012, *Monthly Notices of the Royal Astronomical Society*, 420, L48
- Nalewajko K., Sikora M., Begelman M. C., 2014, *Astrophysical Journal Letters*, 796, L5
- Padovani P., Giommi P., 1995, *Astrophysical Journal*, 444, 567
- Paltani S., Türler M., 2003, *Astrophysical Journal*, 583, 659
- Paltani S., Türler M., 2005, *Astronomy & Astrophysics*, 435, 811
- Peterson B. M. et al., 2004, *Astrophysical Journal*, 613, 682
- Petropoulou M., Arfani D., Mastichiadis A., 2013, *Astronomy & Astrophysics*, 557, A48
- Petropoulou M., Dimitrakoudis S., Padovani P., Mastichiadis A., Resconi E., 2015, *Monthly Notices of the Royal Astronomical Society*, 448, 2412
- Petropoulou M., Mastichiadis A., 2012, *Monthly Notices of the Royal Astronomical Society*, 426, 462
- Petropoulou M., Mastichiadis A., 2015, *Monthly Notices of the Royal Astronomical Society*, 447, 36
- Potter W. J., Cotter G., 2013, *Monthly Notices of the Royal Astronomical Society*, 431, 1840
- Poutanen J., Stern B., 2010, *Astrophysical Journal Letters*, 717, L118
- Pushkarev A. B., Hovatta T., Kovalev Y. Y., Lister M. L., Lobanov A. P., Savolainen T., Zensus J. A., 2012, *Astronomy & Astrophysics*, 545, A113
- Rani B., Lott B., Krichbaum T. P., Fuhrmann L., Zensus J. A., 2013, *Astronomy & Astrophysics*, 557, A71
- Rybicki G. B., Lightman A. P., 1986, *Radiative Processes in Astrophysics*
- Saito S., Stawarz Ł., Tanaka Y. T., Takahashi T., Madejski G., D'Ammando F., 2013, *Astrophysical Journal Letters*, 766, L11
- Savolainen T., Wiik K., Valtaoja E., Tornikoski M., 2008, in *Astronomical Society of the Pacific Conference Series*, Vol. 386, *Extragalactic Jets: Theory and Observation from Radio to Gamma Ray*, Rector T. A., De Young D. S., eds., p. 451
- Sikora M., Begelman M. C., Madejski G. M., Lasota J.-P., 2005, *Astrophysical Journal*, 625, 72
- Sikora M., Begelman M. C., Rees M. J., 1994, *Astrophysical Journal*, 421, 153

- Sikora M., Stawarz Ł., Moderski R., Nalewajko K., Madejski G. M., 2009, *Astrophysical Journal*, 704, 38
- Sironi L., Petropoulou M., Giannios D., 2015, *Monthly Notices of the Royal Astronomical Society*, 450, 183
- Soldi S. et al., 2008, *Astronomy & Astrophysics*, 486, 411
- Stawarz Ł., 2004, *Astrophysical Journal*, 613, 119
- Stecker F. W., 1968, *Physical Review Letters*, 21, 1016
- Stecker F. W., 2013, *Physical Review D*, 88, 047301
- Stern B. E., Poutanen J., 2014, *Astrophysical Journal*, 794, 8
- Tavecchio F., Ghisellini G., Bonnoli G., Ghirlanda G., 2010, *Monthly Notices of the Royal Astronomical Society*, 405, L94
- Tavecchio F., Ghisellini G., Guetta D., 2014, *Astrophysical Journal Letters*, 793, L18
- Tchekhovskoy A., Narayan R., McKinney J. C., 2011, *Monthly Notices of the Royal Astronomical Society*, 418, L79
- Urry C. M., Padovani P., 1995, *PASP*, 107, 803
- Vasudevan R. V., Fabian A. C., 2009, *Monthly Notices of the Royal Astronomical Society*, 392, 1124
- Vlahakis N., Königl A., 2004, *Astrophysical Journal*, 605, 656
- Zacharias M., 2015, *Monthly Notices of the Royal Astronomical Society*, 447, 2021
- Zdziarski A. A., Böttcher M., 2015, *Monthly Notices of the Royal Astronomical Society*, 450, L21
- Zdziarski A. A., Sikora M., Pjanka P., Tchekhovskoy A., 2014, *ArXiv e-prints*